UC Davis
UC Davis Previously Published Works

Title

A Low-Cost System for Measuring Horizontal Winds from Single-Engine Aircraft

Permalink

https://escholarship.org/uc/item/5q93352n

Journal

Journal of Atmospheric and Oceanic Technology, 31(6)

ISSN

0739-0572

Authors

Conley, Stephen A
Faloona, Ian C
Lenschow, Donald H
et al.

Publication Date

2014-06-01

DOI

10.1175/jtech-d-13-00143.1

Peer reviewed

A Low-Cost System for Measuring Horizontal Winds from Single-Engine Aircraft

STEPHEN A. CONLEY AND IAN C. FALOONA

Department of Land, Air and Water Resources, University of California, Davis, Davis, California

DONALD H. LENSCHOW

National Center for Atmospheric Research,* Boulder, Colorado

ANNA KARION AND COLM SWEENEY

University of Colorado Boulder, and NOAA/ESRL, Boulder, Colorado

ABSTRACT

The implementation and accuracy of a low-rate (~1 Hz) horizontal wind measurement system is described for a fixed-wing aircraft without modification to the airframe. The system is based on a global positioning system (GPS) compass that provides aircraft heading and a ground-referenced velocity, which, when subtracted from the standard true airspeed, provides estimates of the horizontal wind velocity. A series of tests was performed flying ''L''-shaped patterns above the boundary layer, where the winds were assumed to be horizontally homogeneous over the area bounded by the flight (approximately 25 km^2). Four headings were flown at each altitude at a constant airspeed. Scaling corrections for both heading and airspeed were found by minimizing the variance in the 1-s wind measurements; an upper limit to the error was then computed by calculating the variance of the corrected wind measurements on each of the four headings. A typical uncertainty found in this manner tends to be less than 0.2 m s^{-1}. The measurement system described herein is inexpensive and relatively easy to implement on single-engine aircraft.

1. Introduction

Atmospheric winds have been measured from multi-engine aircraft for decades. An early way to estimate the wind was by combining the estimated aircraft drift angle (i.e., the difference between the magnetic heading on the compass and the actual ground track determined by visually identifying land marks during the flight) with the true airspeed (TAS) (Card 1919). Subsequently, a variety of approaches have been used incorporating an extensive array of sensors, including accelerometers, global positioning systems (GPS), Doppler navigation systems, inertial navigation systems (INS), and free and

rate gyros to measure the airplane velocity and orientation, and multiport pressure sensors and vanes to measure airspeed and flow angles. Doppler navigation systems were used prior to INS and GPS to estimate the aircraft velocity relative to the ground. These systems used the Doppler shift of four beams transmitted to the left, right, front, and rear and were subject to errors if the beams were reflected by anything other than the ground (e.g., rain or surface water) (Fujita 1966; Lenschow 1970). INS uses gyroscopes for determining the angular orientation (attitude) and integrated accelerometer outputs to determine the airplane velocity and position (Lenschow and Spyers-Duran 1989).

Bonin et al. (2013) describe three methods for determining winds from unmanned aerial vehicle (UAVs). All three methods require a specific flight path optimized for wind determination and are not ideally suited for flights where wind is necessary but not the central objective (e.g., estimating trace gas fluxes). Here, we are concerned solely with a mean horizontal wind

Corresponding author address: Stephen Conley, Department of Land, Air and Water Resources, University of California, Davis, 1 Shields Avenue, Davis, CA 95616.
E-mail: saconley@ucdavis.edu

measurement observed during steady, level flight, which greatly relaxes some of the difficulties of the measurement (variations of angle of attack, pitch, etc.) We point out that there have been other airborne systems developed to also measure turbulence, but these systems required significant modifications to the basic airframe, such as the installation of booms (Crawford and Dobosy 1992) or wing pods (Wood et al. 1997), or the installation of pressure ports on the aircraft nose (Brown et al. 1983). While turbulence would be a desirable additional measurement, what we describe here is a system that requires no modification to the basic airframe and measures accurate mean horizontal winds.

Aircraft certification standards are set by the Federal Aviation Administration (FAA) and require a significant investment of time and capital to modify a certified aircraft. In particular, external airframe modifications (booms, pressure spheres, etc.) require engineering support (to verify aircraft safety is not compromised) and flight testing before FAA approval will be given. Here, we propose a system that can add the capability to measure low-rate (~1 min) horizontal winds from certified aircraft without airframe modifications. Given the comparatively low cost of conducting airborne research from certified single-engine airplanes, this capability represents an unprecedented opportunity to estimate surface emissions of trace gasses (Karion et al. 2013). Additionally, in the time critical period after unexpected disasters (i.e., oil spills, volcanic eruptions, nuclear reactor incidents), this system provides a mechanism to rapidly deploy a reliable wind system on a wide range of certified aircraft. The GPS used here can be completely portable, meaning that any airplane with an air data computer is a candidate for this system.

2. Methods

a. Vector method

In the absence of wind, the velocity of the airplane with respect to the surrounding air v_a and the velocity of the airplane with respect to the ground v_g would be identical. In the case of an air mass moving with respect to the ground (i.e., wind), v_g will differ from v_a by an amount equal to the wind v_w (observed with respect to the ground, and here we neglect the vertical air velocity), that is, $v_g = v_a + v_w$. Once airborne, the airplane has no connection to the earth's surface, conducting its way through the air. The two reference frames are shown in Fig. 1; in the airplane's reference frame (x axis aligned with the longitudinal axis of the airplane) in the absence of sideslip, the wind is simply TAS, that is, $v_a = (\text{TAS}, 0)$.
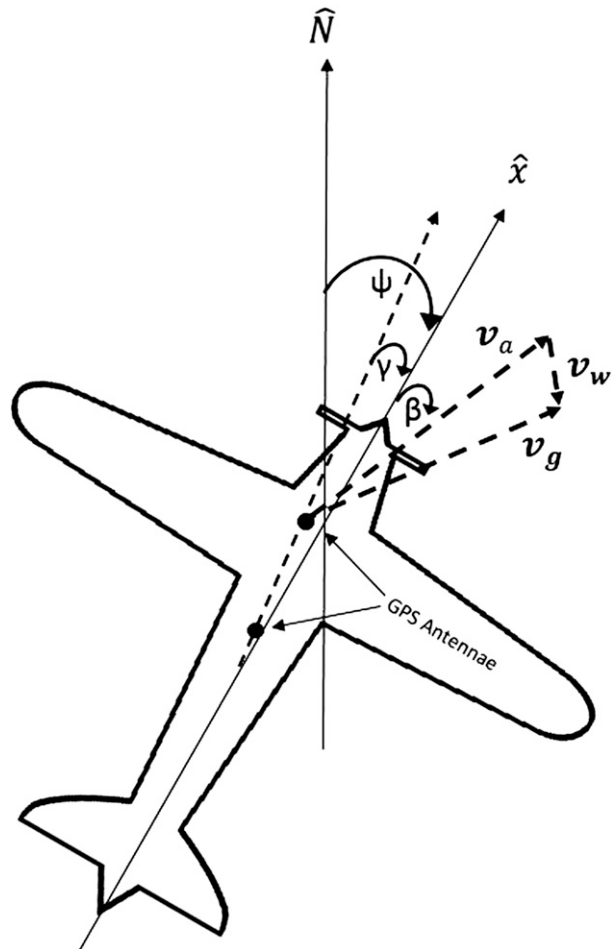

FIG. 1. Reference frames and orientation angles of the aircraft wind measurement system. The velocity of the aircraft through the air v_a is not necessarily aligned with its longitudinal axis x, but translates through the air at a sideslip angle β. Moreover, the axis of the two GPS antennas is not aligned with the longitudinal axis of the aircraft, but it is at a fixed angle γ. True heading ψ is the angle between the aircraft longitudinal axis and geodetic, or true north. The "effective" heading combines β, γ and ψ into one heading that represents the aircraft's motion through the air. The velocity of the aircraft with respect to the earth v_g is simply the sum of the wind v_w and v_a.

Since the airplane flies with an unmeasured angle of sideslip β, the two-dimensional true air velocity includes a small crosswind component, that is,

$$(v_{ax}, v_{ay}) = [\text{TAS}\cos(\beta), \text{TAS}\sin(\beta)]. \quad (1)$$

To transform v_a from airplane coordinates to ground-relative coordinates (v'_{ax}, v'_{ay}), we perform the transformation using ψ, the true heading:

$$v'_{ax} = v_{ax}\sin(\psi) - v_{ay}\cos(\psi)$$
$$v'_{ay} = v_{ax}\cos(\psi) + v_{ay}\sin(\psi). \quad (2)$$

Substituting in the true air velocity for (u,v) leaves

$$
\begin{aligned}
v'_{ax} &= \text{TAS}\cos(\beta)\sin(\psi) - \text{TAS}\sin(\beta)\cos(\psi) \\
&= \text{TAS}\sin(\psi - \beta) \\
v'_{ay} &= \text{TAS}\cos(\beta)\cos(\psi) + \text{TAS}\sin(\beta)\sin(\psi) \\
&= \text{TAS}\cos(\psi - \beta).
\end{aligned} \tag{3}
$$

Equation (3) shows that the sideslip angle and the fixed angle between the GPS antennas and the aircraft's longitudinal axis (see Fig. 1) can all be combined into one "effective" heading $(\psi - \beta)$, reducing the number of variables to be optimized during the calibration maneuvers. Once v_a is known, the wind $(\mathbf{u} = u\hat{x} + v\hat{y})$ is given by

$$
\begin{aligned}
u &= v_{gx} - v_{ax} \\
v &= v_{gy} - v_{ay},
\end{aligned} \tag{4}
$$

where $\hat{x}$ and $\hat{y}$ are unit vectors oriented to the east and north, respectively. In principle, calculation of v_a requires knowledge of the heading, sideslip, bank, and pitch, which requires the installation of additional equipment. Here, we limit the wind calculation to periods of straight and level flight, and assume that variations in bank and pitch can be averaged out on time scales larger than the turbulent eddies through which the airplane flies. Traditional low-cost navigation systems use the earth's magnetic field to estimate the aircraft heading and then apply the local magnetic variation to estimate the aircraft heading referenced to true north. With careful calibration, the magnetic heading can be determined with a solid-state magnetic compass to within about 1° (Markovic et al. 2011). For an airplane traveling at $60\,\text{m s}^{-1}$, that error translates into a $1\,\text{m s}^{-1}$ error in the lateral wind component (i.e., $60\,\text{m s}^{-1} \times \sin 1°$). A GPS compass uses dual antennas on a single GPS receiver, allowing the heading (obtained from two displaced antennas) to be measured within 0.1° (Hemisphere GPS 2011).

Scientific Aviation operates a 1998 Mooney M20M TLS that has been modified for atmospheric research with three air inlets mounted outboard on the starboard wing, a Vaisala HMP60 temperature/humidity sensor, a Hemisphere VS101 differential GPS, and an Aspen Avionics PFD1000 primary flight display (PFD), along with a Mid-Continent TI1200 1.2-kW power inverter. The heading error in the GPS is a function of antenna separation distance, and the antennas on the top of the Mooney's fuselage are 179 cm apart, resulting in a stated error of 0.11°. This aircraft was chosen because of its desirable research capabilities; it can fly as high as 8 km, as fast as $100\,\text{m s}^{-1}$ and as slow as $40\,\text{m s}^{-1}$, and with 336 L of usable fuel, it can remain airborne for more

than 6 h. The PFD provides true airspeed and altitude at a 1-Hz sample rate over an RS232 serial interface. Airspeed is measured via a standard Pitot-static tube at the leading edge of the left wing.

A correction to the ground-relative velocity must be made for the combination of β and the offset of the GPS-measured heading because neither the aircraft velocity relative to the air nor the two GPS antennas are exactly aligned with the longitudinal axis of the airplane (see Fig. 1). Rather than attempting to measure the sideslip angle, which can vary based on the rudder setting, we perform calibration maneuvers with a fixed rudder trim setting to calculate the heading correction for the given airspeed. True airspeed is not directly measured, but can be easily calculated given the indicated airspeed (IAS), temperature, and static pressure (McCormick 1979; Wendisch and Brenguier 2013).

Position and velocity from the GPS along with avionics data (airspeed, rate of turn, and vertical speed) from the PFD were recorded at 1 Hz. For the calibration maneuver, we selected periods when the airplane was in straight and level flight; that is, the data were excluded when the rate of turn exceeded $1°\,\text{s}^{-1}$ or the vertical speed (rate of climb/descent) exceeded $3\,\text{m s}^{-1}$.

The calibration maneuver relies on the fact that a bias in the effective heading or airspeed will result in a wind estimate that varies with the heading. For example, if the measured airspeed is biased high, the leg into the wind will yield a longitudinal wind component that is larger than the actual wind, while a leg with the wind will yield a measured component that is smaller than the actual wind component. Heading errors are similarly manifested. This allows us to determine the optimal offset to both the heading and airspeed. Using a series of four orthogonal headings, we calculate the heading offset (plus/minus degrees) and the airspeed correction (multiplicative factor) that minimizes the sum of the squares between the individual 1-s wind component samples and the mean wind calculated over all eight legs. This is done by iteration by varying the heading offset from $-3°$ to $+3°$ (increments of 0.06°) and the airspeed correction from -2% to $+5\%$ (increments of 0.07%) until the combination with the smallest deviation was found.

b. Error analysis

We have shown earlier that uncertainties in v_g obtained from the GPS are insignificant compared to errors in v_a We assume the true wind component u_w is equal to the measured wind u_m plus some correction term u_c, that is,

$$
u_w = u_m + u_c. \tag{5}
$$

TABLE 1. Calibration maneuver (L pattern) over BAO tower in Erie. Fields are the true heading flown by the airplane, calculated components of the wind (U, V) with the std dev of the measurements during the leg, the calculated wind direction (also true), wind speed, and the length of the leg. The all measurements row shows the mean of the 1-s measurements for all of the data and the root-mean-square (RMS) of the std dev of each of the leg means. The standard deviation quoted on the leg mean row indicates the actual std dev of the eight components measured for the different headings.

Heading	U (m s^{-1})	V (m s^{-1})	Direction (°)	Speed (m s^{-1})	Leg time (s)
189	−2.8 ±1.1	−0.5 ±1.4	79.2	2.9	176
283	−2.9 ±1.2	−0.1 ±1.5	88.3	3.0	91
098	−2.6 ±1.6	0.4 ±1.4	97.8	2.6	156
015	−3.1 ±1.4	0.0 ±1.2	90.8	3.1	137
190	−2.6 ±1.2	0.6 ±1.2	102	2.6	165
285	−3.0 ±1.2	−0.8 ±1.4	75.9	3.1	140
098	−2.9 ±1.1	−0.3 ±1.4	83.8	2.9	192
014	−2.6 ±1.4	0.9 ±1.2	109.7	2.7	135
190	−2.9 ±1.0	1.2 ±1.2	112.5	3.1	184
All measurements	−2.8 ±1.7	0.15 ±1.8			
Leg mean	−2.8 ±0.18	0.15 ±0.62		2.9 ±0.21	

During the course of the calibration maneuvers (typically eight legs over ~30 min), there is real variation in the wind (both over time and space) and error in the measurement. The variance in the measured wind σ_m^2 is equal to the sum of the variances in the true wind σ_w^2 and the error in the measurement σ_b^2:

$$\sigma_m^2 = \sigma_b^2 + \sigma_w^2. \qquad (6)$$

So, for a given set of legs, the measured variance is actually an upper limit to the variance of the correction term (which is the wind error—that is, the difference between what we measure and the true wind). The results from the individual legs are shown in Tables 1–4. We tried to maintain a constant heading for at least 2 min, recording GPS and navigation data every second. The tables show the estimated wind components (U, V) along with the standard deviation of the 1-s values during each leg. The last two rows of each table show the mean and standard deviation of the calculated wind components during the entire maneuver (all four headings) and the mean and standard deviation of the eight leg means, which provide an estimate of the error in the method.

3. Test Cases

a. Case 1—Erie, Colorado

To estimate the measurement error, we flew a series of "L"-shaped legs and compared the wind measured on each of the four headings (two outbound, two inbound). The first such test was performed on 31 May 2012, over Erie, Colorado. During the flight, clear skies prevailed with a temperature of 21°C and there was no significant weather in the area. The location was chosen because of its proximity to the National Oceanic and Atmospheric Administration (NOAA) Boulder Atmospheric Observatory (BAO) tower (Kaimal and Gaynor 1983), which has a 2D sonic anemometer at 300 m above ground level (AGL) [1884 m above mean sea level (MSL)] measuring horizontal winds. Eight legs were flown at a mean altitude of 2016 m MSL (132 m above the anemometer) as shown in Table 1. Using the

TABLE 2. The L pattern flown over Arcata, CA, at 5344 m. Calculations as described in Table 1.

Heading	U (m s^{-1})	V (m s^{-1})	Direction (°)	Speed (m s^{-1})	Leg time (s)
349	12.1 ±0.2	−28.5 ±0.2	337.0	31.0	125
079	11.3 ±0.3	−29.6 ±0.3	339.1	31.6	85
168	11.4 ±0.2	−29.5 ±0.1	338.9	31.7	95
349	11.4 ±0.3	−29.7 ±0.2	339.0	31.8	119
260	11.6 ±0.3	−29.1 ±0.3	338.2	31.3	122
078	11.7 ±0.3	−28.7 ±0.4	337.9	31.0	113
260	11.8 ±0.2	−29.8 ±0.2	338.5	32.0	118
348	11.7 ±0.2	−29.5 ±0.4	338.4	31.8	120
All measurements	11.6 ±0.3	−29.3 ±0.3			
Leg mean	11.6 ±0.23	−29.3 ±0.45		31.5 ±0.38	

TABLE 3. The L pattern flown over Arcata at 3271 m. Calculations as described in Table 1.

Heading	U (m s^{-1})	V (m s^{-1})	Direction (°)	Speed (m s^{-1})	Leg time (s)
168	5.0 ±0.1	−22.3 ±0.7	347.5	22.9	120
259	5.0 ±0.2	−22.3 ±0.4	347.4	22.8	123
079	5.0 ±0.2	−22.2 ±0.4	347.2	22.7	126
350	5.1 ±0.2	−21.2 ±0.5	346.6	21.8	127
169	4.9 ±0.1	−21.8 ±0.2	347.4	22.3	112
259	5.0 ±0.2	−23.5 ±0.7	347.9	24.0	119
349	5.1 ±0.2	−24.2 ±0.2	348.2	24.7	129
078	5.0 ±0.2	−22.9 ±0.3	347.6	23.4	121
All measurements	5.0 ±0.2	−22.5 ±0.5			
Leg mean	5.0 ±0.06	−22.5 ±0.87		23.1 ±0.23	

optimization described in the preceding section, the optimal corrections were found to be −0.9° for the heading and +2.4% for the airspeed at a cruise speed of 61 m s^{-1}.

Variability in the actual wind was large, as evidenced by the spread in the 1-s measurements along a constant heading (∼1.7 m s^{-1} standard deviation). There is also large variability in the 2-min averages, particularly in V. During that same period, the standard deviation of the 30-s measurements taken on the BAO tower was 1.1 m s^{-1} for U and 1.2 m s^{-1} for V. For a wind of roughly 2 m s^{-1}, the 30-s averaged measurement on the tower covers a spatial extent of approximately 60 m, similar to the 1-s airplane measurement. We note that the standard deviation in the 2-min averages (individual legs) is reduced to 0.2 m s^{-1} for U and 0.6 m s^{-1} for V over the entire 23 min of data.

While the aircraft was in the vicinity of the BAO tower, winds averaged 275° at 2.8 m s^{-1} from the aircraft and 298° at 1.8 m s^{-1} from the tower. Figure 2 shows the spatial variability of the measured winds measured from the airplane. When the airplane was closest to the tower (within 2 km), airplane winds averaged 302° at 2.0 m s^{-1}. For a sample of 86 s with a boundary layer height z_i and an integral length scale $l = 0.5z_i$ (Lenschow and Stankov 1986), we expect the mean squared

deviation between the sample mean and the ensemble mean to be

$$\overline{(u^T - \overline{u})^2} = 2\frac{\overline{u^2}l}{L}, \qquad (7)$$

where $\overline{u^2}$ is the ensemble variance, and L is the sampling length (5256 m), and u^T is the sample mean (Lenschow et al. 1994). The boundary layer height, estimated from aircraft profiles by identifying the inflection points in potential temperature and relative humidity, was 1350 m, thus, $l = 675$ m. Aligning the coordinate system with the mean wind and using the observed variance of the tower-measured longitudinal wind (1.6 m^2 s^{-2}) as an estimate of the ensemble variance, the estimated standard deviation of the measured boundary layer wind is ∼0.62 m s^{-1}. The averaged wind components for the 86 s within 2 km of the tower were −1.8 and 1.1 m s^{-1} while the tower averages were −1.6 and 0.9 m s^{-1}, well within the estimated variance. We also note that some of the difference between the tower and the aircraft can be attributed to the difference in altitude (132 m) between the anemometer and the flight path.

b. Case 2—Trinidad Head, California

The second test flight was conducted on 12 January 2013, over Trinidad Head on the north coast of

TABLE 4. The L pattern over Sacramento at 1127 m. Calculations as described in Table 1.

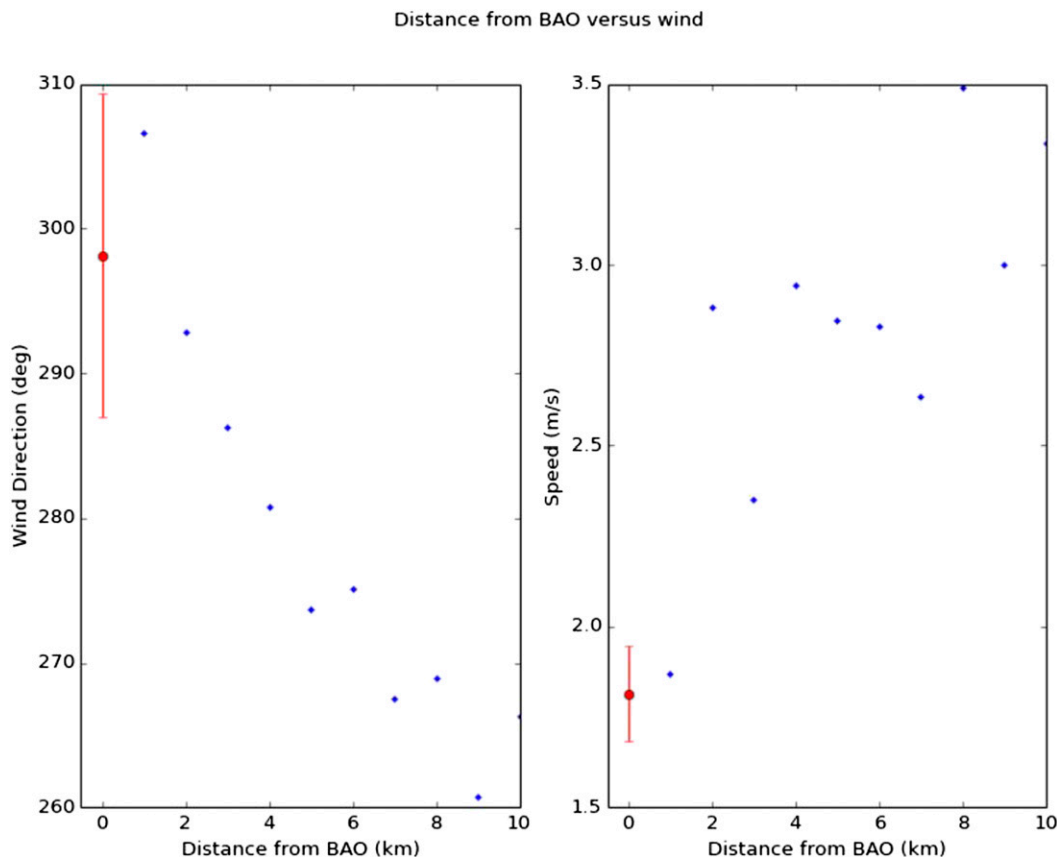| Heading	U (m s^{-1})	V (m s^{-1})	Direction (°)	Speed (m s^{-1})	Leg time (s)
105	−3.8 ±0.2	4.2 ±0.1	138.0	5.6	134
018	−4.1 ±0.2	5.1 ±0.3	141.1	6.5	127
194	−3.7 ±0.2	5.0 ±0.2	143.2	6.2	133
287	−3.4 ±0.2	4.6 ±0.1	143.0	5.7	118
105	−3.4 ±0.1	4.8 ±0.1	144.9	5.9	136
018	−3.5 ±0.1	5.1 ±0.2	145.6	6.1	121
194	−3.4 ±0.1	4.7 ±0.3	143.6	5.8	148
287	−3.6 ±0.2	4.7 ±0.1	143.1	5.9	170
All measurements	−3.6 ±0.2	4.8 ±0.2			
Leg mean	−3.6 ±0.2	4.8 ±0.3		6.0 ±0.29	

Distance from BAO versus wind

FIG. 2. Wind direction and speed as a function of distance from the BAO tower. The winds in the vicinity of the tower were not horizontally homogeneous. While the average aircraft wind during the maneuver differed significantly from the tower, if the comparison is limited to when the aircraft was within 2 km of the tower, then the two agree to within $0.2\,\mathrm{m\,s^{-1}}$. The red circle and line show the mean wind measured at the BAO tower and the standard error of the mean for the entire period of the maneuver.

California during a routine flight performed monthly for the Global Monitoring Division of NOAA. The flight was conducted approximately 10 km offshore with broken to overcast skies, a temperature of 7.2°C, and occasional periods of light precipitation below the flight level. Two sets of legs were flown, the first at 5344 m MSL (Table 2) and the second at 3271 m (Table 3). At each altitude, we flew several legs into and away from the wind direction as well as crosswind. For the first set of legs, the optimum correction was −1.3° for the heading and +2.6% for the airspeed. For the second set of legs, the optimum corrections were −1.4°/+2.5%, very similar to the values found at the higher altitude and those derived from the Colorado tests.

Both altitudes were well above the marine boundary layer (MBL) top and yet the higher altitude (5344 m) showed significantly less leg-to-leg deviation than the lower leg (3271 m). The same was true of the variance in the 1-s measurement within each of the 2-min legs. For the eight low-altitude legs, the standard deviation of the

V component ranged from 0.2 to $0.7\,\mathrm{m\,s^{-1}}$ with a mean of $0.42\,\mathrm{m\,s^{-1}}$, while at the higher altitude, the range was from 0.1 to $0.4\,\mathrm{m\,s^{-1}}$ with a mean of $0.26\,\mathrm{m\,s^{-1}}$.

c. Case 3—Sacramento, California

The third test was performed on 1 February 2013, just south of Sacramento, California (Table 4). Conditions for the flight included clear skies, calm surface winds, and no significant weather. For this test, the airplane climbed above the boundary layer to a height of 1127 m MSL and flew eight legs of roughly 2 min each, on the four cardinal headings (north, south, east, west). Winds at that altitude were very consistent as seen in Table 4; the variability in the leg-averaged winds is $\sim0.2\,\mathrm{m\,s^{-1}}$. The standard deviation of the 1-s values on each leg varied between 0.1 and $0.2\,\mathrm{m\,s^{-1}}$ for U and between 0.1 and $0.3\,\mathrm{m\,s^{-1}}$ for V. The standard deviation of the wind components calculated from the eight legs was $0.2\,\mathrm{m\,s^{-1}}$ for both U and V.
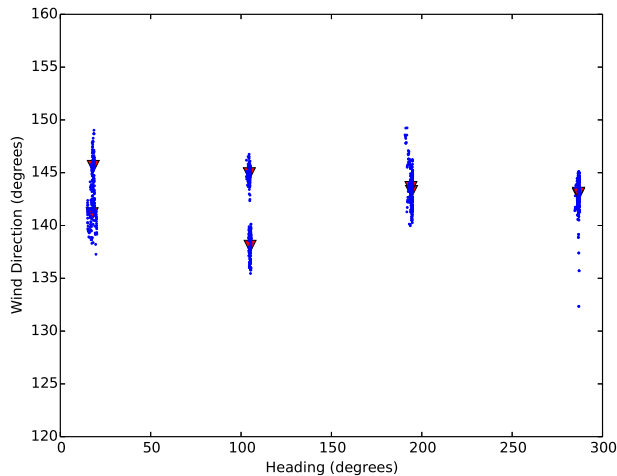
FIG. 3. Sacramento flight (1 Feb 2013). Plot shows aircraft heading on the horizontal axis and calculated wind direction on the vertical axis. Blue dots represent 1-s data, while the red triangles show the mean values for the individual legs.

To gain confidence in the aircraft-derived winds, we looked for a correlation between the heading and the measured wind, as shown in Fig. 3. Any correlation between the measured wind and the aircraft heading is an indication that the winds may not be calculated correctly. For headings that span the circle, wind directions vary between 138° and 146° for the leg averages. The standard deviation of the wind directions (1-s data over all eight legs) is only 2.9°. Performing a linear regression (least squares) of the heading and wind direction, the R^2 value is only 0.005, suggesting no correlation.

d. Case 4—Dallas, Texas

The final test of the system was performed during sampling flights near Dallas, Texas, on 27 March 2013. A high-resolution Doppler lidar (HRDL) operated by the NOAA Earth System Research Laboratory (ESRL) Chemical Sciences Division was deployed at the National Weather Service site in Fort Worth, Texas (Grund et al. 2001). It continuously measured horizontal winds from 12 to 1600 m AGL in scans every 20 min. Figure 4 shows the comparison between the aircraft and HRDL measurements at the approximate aircraft altitude (~760 m AGL). One issue with comparing these systems is that the aircraft was sampling an area 200–300 km wide, while the HRDL was continuously measuring winds in conical scans within a few kilometers of the site. Looking at the periods when the airplane was within 50 km of the HRDL, the average deviation between the HRDL and the airplane is 0.5 ± 1.4 m s^{-1}, and 2.7° ± 4.7° for wind direction. To get an idea of the "expected" variability between the HRDL and the airplane, we examine the HRDL wind variability in time and use Taylor's "frozen turbulence" hypothesis (Willis and Deardorff 1976) to estimate how it varies in space. The dark blue dots show the period when the airplane was closest to the HRDL (~30 km); during this time the wind speed at the HRDL is ~12 m s^{-1}, suggesting a transit time of ~41 min. Between 1900 and 2000 UTC, the HRDL wind speed increased from ~10 to ~13 m s^{-1}, which would suggest a 2 m s^{-1} difference at 30 km is not
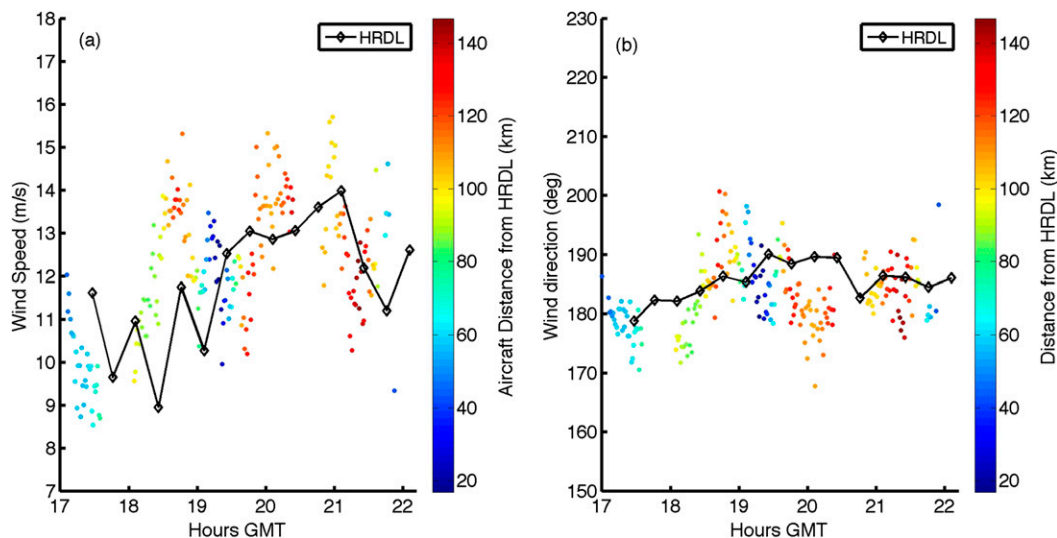

FIG. 4. Comparison of wind (a) speed and (b) direction measured from the aircraft with those measured on the ground by HRDL. The 20-min average HRDL winds (black diamonds) for the approximate average aircraft flight altitude (~760 m AGL) are shown vs the 1-min average of the winds from the aircraft system during level flight segments. The aircraft wind points are colored according to the distance of the aircraft from the location of HRDL.

TABLE 5. Rudder sensitivity test. To make the lateral component comparable between legs with slightly different headings, the wind vector is rotated to the heading of the first leg (with the rudder centered). These results demonstrate the importance of consistent rudder trim, as the wind direction changes by 46° from full right to full left rudder trim.

Position	U (m s^{-1})	V (m s^{-1})	Lateral (m s^{-1})	Heading	Direction (°)	Speed (m s^{-1})	Leg time (s)
Centered	−1.7	4.4	−0.7	348.1	159.1	4.7	54
Left	1.2	5.5	2.3	339.3	192.5	5.6	98
Right	−2.6	3.9	−1.7	343.6	146.5	4.6	102
Std dev	1.62	0.67					

unexpected at that time of day. Furthermore, this experiment was performed without a dedicated calibration maneuver; instead, we used the corrections measured in Sacramento (−0.7°, +2.6%).

e. Case 5—Rudder sensitivity test

Slight variations in rudder trim setting (a pilot adjustment) will affect the heading correction and hence the wind solution. To investigate the dependence of the wind calculation on the rudder trim, we established the airplane in level cruise above the boundary layer and flew 1-min legs with the rudder trim in various positions. To eliminate any dependence on wind speed, we examine the lateral component U_l of the wind in the airplane's initial reference frame (rudder trim centered), given by

$$U_l = u \cos(\psi) - v \sin(\psi), \qquad (8)$$

where u and v are the east and north components of the wind, respectively, and ψ is the aircraft heading. The results shown in Table 5 indicate a spread of 4 m s^{-1} from full left deflection to full right deflection of the rudder. For a 5 m s^{-1} wind, this translates into an error of 30° in the wind direction if the rudder trim is set to full left or right deflection, rather than centered. Given the sensitivity of the wind estimate on the trim setting, it is essential that the trim setting used during the calibration maneuvers is maintained during periods of wind measurements.

4. Conclusions

Horizontal winds can be measured accurately from small single-engine airplanes without any airframe modifications, and using only equipment approved for flight by the U.S. Federal Aviation Administration (FAA). The accuracy of the system is estimated using two sets of four orthogonal 2-min legs. During steady winds (e.g., Sacramento test), the standard deviation of the wind components estimated with this method was less than 0.3 m s^{-1}, which we determined is an upper limit on the error. Winds measured from the aircraft were also compared to the NOAA BAO tower, and

when the airplane was within 2 km of the tower, winds agreed to better than 0.3 m s^{-1} in each component.

Further investigation is needed to estimate the accuracy of the wind measurement when the airplane is turning or climbing/descending. Further enhancements to the accuracy could be achieved by replacing the TAS reported by the Aspen (0.5 m s^{-1} resolution) with a higher-resolution pressure transducer.

REFERENCES

Bonin, T. A., P. B. Chilson, B. S. Zielke, P. M. Klein, and J. R. Leeman, 2013: Comparison and application of wind retrieval algorithms for small unmanned aerial systems. *Geosci. Instrum. Methods Data Syst.,* **2,** 177–187, doi:10.5194/gi-2-177-2013.

Brown, E. N., C. A. Friehe, and D. H. Lenschow, 1983: The use of pressure fluctuations on the nose of an aircraft for measuring air motion. *J. Climate Appl. Meteor.,* **22,** 171–180, doi:10.1175/1520-0450(1983)022<0171:TUOPFO>2.0.CO;2.

Card, S., 1919: *Air Navigation: Notes and Examples.* E. Arnold, 140 pp.

Crawford, T. L., and R. J. Dobosy, 1992: A sensitive fast-response probe to measure turbulence and heat flux from any airplane. *Bound.-Layer Meteor.,* **59,** 257–278, doi:10.1007/BF00119816.

Fujita, T., 1966: Accurate calibration of Doppler winds for their use in computation of mesoscale wind fields. *Mon. Wea. Rev.,* **94,** 19–35, doi:10.1175/1520-0493(1966)094<0019:ACODWF>2.3.CO;2.

Grund, C. J., R. M. Banta, J. L. George, J. N. Howell, M. J. Post, R. A. Richter, and A. M. Weickmann, 2001: High-resolution Doppler lidar for boundary layer and cloud research. *J. Atmos. Oceanic Technol.,* **18,** 376–393, doi:10.1175/1520-0426(2001)018<0376:HRDLFB>2.0.CO;2.

Hemisphere GPS, 2011: VS101 and VS111 GPS compass: User guide. Part No. 875-0253-00 Rev B1, 60 pp. [Available online at www.hemgps.com/dl/875-0253-000_A1(MNL,UG,VS101-111)_web.pdf.]

Kaimal, J. C., and J. E. Gaynor, 1983: The Boulder Atmospheric Observatory. *J. Climate Appl. Meteor.,* **22,** 863–880, doi:10.1175/1520-0450(1983)022<0863:TBAO>2.0.CO;2.

Karion, A., and Coauthors, 2013: Methane emissions estimate from airborne measurements over a western United States

natural gas field. *Geophys. Res. Lett.,* **40,** 4393–4397, doi:10.1002/grl.50811.

Lenschow, D. H., 1970: Airplane measurements of planetary boundary layer structure. *J. Appl. Meteor.,* **9,** 874–884, doi:10.1175/1520-0450(1970)009<0874:AMOPBL>2.0.CO;2.

——, and B. B. Stankov, 1986: Length scales in the convective boundary layer. *J. Atmos. Sci.,* **43,** 1198–1209, doi:10.1175/1520-0469(1986)043<1198:LSITCB>2.0.CO;2.

——, and P. Spyers-Duran, 1989: Measurement techniques: Air motion sensing. NCAR RAF Bull. 23, 36 pp. [Available online at http://nldr.library.ucar.edu/repository/assets/atd/ATD-000-000-000-062.pdf.]

——, J. Mann, and L. Kristensen, 1994: How long is long enough when measuring fluxes and other turbulence statistics. *J. Atmos. Oceanic Technol.,* **11,** 661–673, doi:10.1175/1520-0426(1994)011<0661:HLILEW>2.0.CO;2.

Markovič, R., A. Krajnc, and D. Matko, 2011: Calibration of a solid-state magnetic compass using angular-rate information from low-cost sensors. *IET Sci. Meas. Technol.,* **5,** 54–58, doi:10.1049/iet-smt.2010.0050.

McCormick, B. W., 1979: *Aerodynamics, Aeronautics, and Flight Mechanics.* John Wiley & Sons, Inc., 652 pp.

Wendisch, M., and J. Brenguier, 2013: *Airborne Measurements for Environmental Research.* Wiley-VCH, 655 pp.

Willis, G. E., and J. W. Deardorff, 1976: On the use of Taylor's translation hypothesis for diffusion in the mixed layer. *Quart. J. Roy. Meteor. Soc.,* **102,** 817–822, doi:10.1002/qj.49710243411.

Wood, R., I. M. Stromberg, P. R. Jonas, and C. S. Mill, 1997: Analysis of an air motion system on a light aircraft for boundary layer research. *J. Atmos. Oceanic Technol.,* **14,** 960–968, doi:10.1175/1520-0426(1997)014<0960:AOAAMS>2.0.CO;2.